Performance of the oxide film of pure aluminium processed by WEDM-HS

Dongjie Cheng[1], *Guangfeng Shi*[1] ✉, *Guoquan Shi*[2], *Zhe Xu*[1], *Keke Zhu*[1]

[1]*College of Electro-Mechanical Engineering, Changchun University of Science and Technology, 130022 Changchun, People's Republic of China*
[2]*Suzhou Institute of Biomedical Engineering and Technology, Chinese Academy of Science, 215163 Suzhou, People's Republic of China*
✉ *E-mail: shiguangfeng@cust.edu.cn*

Published in Micro & Nano Letters; Received on 12th July 2016; Revised on 1st December 2016; Accepted on 1st December 2016

To study the performance of pure aluminium (Al) oxide film produced by high-speed wire electrical discharge machining (WEDM-HS), some characterisation indices including phase composition, surface morphology characteristics, roughness, friction coefficient, oxide content and thickness of the 1060 Al oxide film are researched, respectively, through X-ray diffraction, energy dispersive X-ray spectroscopy, scanning electron microscope, confocal microscope, contourgraph and nanoindentation. The results show that the produced oxide film of 1060 Al is mainly composed of Al_2O_3 phase after the 1060 Al sample processed by WEDM-HS. With the pulse width of WEDM-HS is gradually decreasing, the Al_2O_3 content values in the oxide film are all more than 84% with slight change. The surface morphology of the oxide film is made up of honeycomb holes of microns size. Moreover, the ladder-like microstructures of square bracket are found for the first time at the inside wall from bottom to top of the microholes. With the decreasing of the pulse width, the thickness and the friction coefficient of the oxide film first decrease, then increase and finally tend to be stable. They both have certain relationships with the Al_2O_3 content of the oxide film.

1. Introduction: Aluminium (Al) is a kind of important material for the industrial applications. It has a relatively high electrical conductivity, thermal conductivity, ductility and reflectivity, non-magnetic, non-low-temperature brittleness and other advantages. However, pure Al has a strong affinity for oxygen in the air so that the newly-exposed Al surface can rapidly form a layer of oxide film with a thickness of 0.005–0.015 μm. Moreover, the oxide film is mainly composed of amorphous hydrate with the result that its hardness, corrosion resistance and wear resistance are not good [1, 2], therefore it cannot meet the requirements of extreme application environment. We must treat the Al surface by some special methods to improve its using performance while overcome its shortcomings. Thus it can be seen, the surface modification methods of pure Al for improving the surface strength and corrosion resistance are significant.

Methods of Al oxidation include anodic oxidation, microarc oxidation [3], electroplated coating [4] and thermal spraying [5] and so on, making the Al oxide film hard and dense to improve its wear resistance and corrosion resistance [6–8]. While some methods such as anodic oxidation [9, 10] need extremely strict conditions but result with thin oxide film and poor compactness. Moreover, the Al oxide film got by microarc oxidation should be thicker for the acceptable performance, so it has its limitations in some special engineering applications requiring the thickness of oxide film below a specified value. Besides, the method of electroplated coating needs some special intermediate processing result with non-uniformity and pollution. Furthermore, the ceramic layer got by thermal spraying is non-uniform, fragile and easy to peel and so on. So the problems above make the application of these methods in industry limited.

After we did some experiments about mechanical rulling on the pure Al samples, we cut the sample by high-speed wire electrical discharge machining (WEDM-HS) to investigate the metallographic phase from the cross section on which the Al oxide film is too hard to be etched off by the general corrosive fluids. To the contrary, another idea of getting the Al oxide film is created. Under the instantaneous high temperature of WEDM-HS, the pure Al is partially melted and oxidised result with a dense layer of Al oxide film at the cut surfaces. And the process is simple and without pollution, so it is a very promising surface modification technology. In this Letter, the technology of WEDM-HS is used to realise the oxide film of pure Al, and its performance is researched.

2. Experiment

2.1. Experimental materials: Industrial 1060 pure Al is used as the experimental materials and its chemical composition is shown in Table 1.

2.2. Experimental methods: Several polished and cleaned blanks of 1060 Al are prepared for the WEDM-HS experiments and Jinma DK7732-type as the WEDM-HS machine is used to process the blanks into samples with different processing parameters. Moreover, each sample dimension is $10 \times 10 \times 5$ mm for convenient processing and testing. In the dielectric fluid of Jiarun JR3A emulsion, the cold-drawn molybdenum wire of 0.18 mm is used as cathode and the 1060 Al blank is used as anode. Moreover, the pulse power supply is unidirectional DC with the no-load voltage of 70 V. The test process parameters are as shown in Table 2. The pulse widths are sequentially reduced from 32 to 4 μs with the ratio 1:7 of pulse interval to pulse width, while the pulse interval, power tube, wire speed, and frequency conversion keep constant. After processed with different pulse widths of WEDM-HS, the oxide films on the cross-section surfaces of the 1060 Al samples are got and prepared for the inlay metallographic form and cleaned by ultrasound with acetone and ethanol.

Then a PANalytical Empyrean X-ray diffraction (XRD) is used to test the phase composition of the 1060 Al oxide film. The test parameters conclude the tube voltage 40 kV, the tube current 40 mA, the scanning speed 6.5°/min, the sample width 0.8°, 2θ range 25°–90°, copper target, Ka-ray radiation, and continuous sampling. Then a Carl Zeiss scanning electron microscope (SEM) with energy dispersive X-ray spectroscopy (EDS) is used to observe the surface morphology characteristics and the spectrum of the 1060 Al oxide film. Moreover, a laser scanning confocal microscope is used to observe the cross-section morphology and measure the thickness of the oxide film. Besides, a Marr contourgraph is used to measure the surface roughness of the sample.

Table 1 Composition of 1060 Al

Composition, %								
Fe	Cu	Si	Mg	Mn	Zn	V	Ti	Al
≤0.40	≤0.05	≤0.25	≤0.05	≤0.05	≤0.05	≤0.05	≤0.03	≥99.6

Finally, a continuous stiffness measurement nanoindentation is used to measure the friction coefficient of the 1060 Al oxide film.

3. Results and discussion

3.1. Phase composition analysis of the oxide film: Al_2O_3 phase compositions are found in the 1060 Al oxide films of seven samples, whose XRD patterns are shown as in Fig. 1. Obviously, the Al_2O_3 phase compositions of the oxide films have no relation to the pulse widths of WEDM-HS. The lattice constants of the measured Al_2O_3 are $a = 4.7500$ Å, $b = 4.7500$ Å and $c = 12.9700$ Å and the density of measured Al_2O_3 is 4.02 g/cm^3. With the pulse widths decreasing, the diffraction intensity peaks of Al_2O_3 phase of different samples have a little change, but the phase composition does not change.

To get further information, the EDS spectra of the oxide film is analysed (Fig. 2). Moreover, the main elements of the oxide film are O and Al. It is also proved that Al_2O_3 in the oxide film is generated during the process of 1060 Al by WEDM-HS.

The content of Al_2O_3 in the oxide film is also got as shown in Fig. 3. With the pulse width decreasing, the Al_2O_3 content first decreases and then increases, but the content change is not obvious. Overall consideration, the Al_2O_3 content of the oxide film is all more than 84%.

3.2. Surface micromorphology analysis of the oxide film: The machining principle of WEDM-HS is to keep the continuous pulse discharge between the wire electrode and the workpiece, and simultaneously form a discharge channel with high temperature to make the materials melted even evaporated. The material of the workpiece will be removed steadily and the honeycomb structure will be formed on the new working surface with a lot of small pits and humps in the end.

In this experiment, the honeycomb structure with microholes on the oxide film is observed by the 200× SEM images as shown in Fig. 4 and the surface of the oxide film in Fig. 4*a* is rough. There are a few small bumps and potholes, the structural arrangement of which is large discrete. Besides the bulky grains composed by 1060 Al and its melted oxide, there are many small grains and microholes. Moreover, the microholes are the discharge channels formed by the process of WEDM-HS. It can be seen from Fig. 3 that the diameter and the depth of the discharge pore decrease with the pulse width decreasing, so that the honeycomb structure is closely arranged with a better surface quality of the oxide film, which has a good wettability and erosion resistance [11–13].

The SEM images of microhole under different magnification factors with the discharge-pulse width 24 µm are as shown in Fig. 5. The honeycomb structure composed by those close together microholes under 1 K× and 2 K× magnifications can be seen from Figs. 5*a* and *b*. With the amplification factor gradually increasing, the morphology of single discharge microhole on the honeycomb structure becomes gradually clear, and the microhole diameter is about 1 µm as shown in Fig. 5*d*. Furthermore, ladder-like microstructures of square bracket are found for the first time at the inside wall from bottom to top of the microhole, because the honeycomb structure as shown in Fig. 3 is common for the process of WEDM-HS of various materials.

WEDM-HS is a continuous process of discharge, breakdown and deionisation. Correspondingly, the workpiece is also in the continuous process of heat and cool. The discharge pulse produces extremely high temperature, which at the discharge channel centre is up to 4000 K. Moreover, the temperature of the bottom is lower than that of the top so that the temperature gradient of the uneven temperature field is formed and then causes the squares of ladder-like distribution to change from small to large along the microhole from bottom to top.

3.3. Analysis of cross-section morphology and film thickness of the oxide films: A laser scanning confocal microscope is used to observe the cross section of the oxide film whose thickness is more than 10 µs, and the structure is compact, as shown in Fig. 6. The combination of Al_2O_3 oxide and 1060 Al belongs to the metallurgical combination, which is very strong and not easy to fall off from the matrix. Black spots in the picture are corrosion pits produced by the 10% hydrofluoric acid solution when cleaning the cross-section surface of the sample after WEDM-HS. Moreover, the area without black spots is just the oxide film, which indirectly proves that the corrosion resistance of the oxide film formed by the process of WEDM-HS is good.

The thickness values of the oxide film under different pulse widths are listed in Table 3. Moreover, the relationship between the thickness of the oxide film and the pulse width is drawn as shown in Fig. 7. The thickness change of the oxide film can be divided into two stages. When the pulse width is not less than 8 µs, the thickness of the oxide film decreases slowly and then decreases rapidly with the pulse width decreasing. When the smallest thickness value 7.7 µm is getting, the thickness of the oxide film increases slowly with the pulse width continues decreasing. By contrast, it is known that the change tendency of the relationship in Fig. 7 is consistent with that in Fig. 3. Thus it can be seen that the thickness of the oxide film is linked with the Al_2O_3 content.

The process parameters of WEDM-HS are decided by the discharge energy of a single pulse during the machining, and the pulse width is the main factor of deciding the single pulse discharge

Table 2 Process parameters

Sample number	Pulse width, µs	Pulse interval, µs	Power tube, (number)	Wire speed, Hz	Frequency conversion, Hz
1	32	224	7	50	25
2	24	168			
3	16	112			
4	12	84			
5	8	56			
6	6	42			
7	4	28			

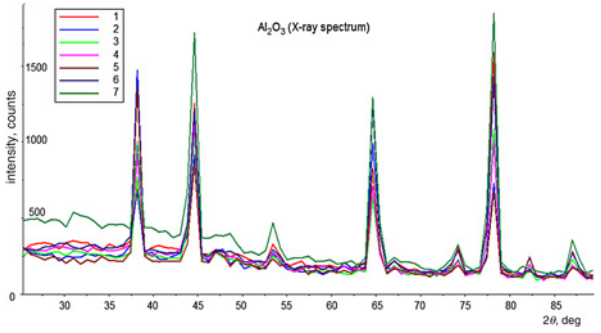

Fig. 1 *XRD spectrum of phase composition of the oxide films obtained under different pulse widths*

doi: 10.1049/mnl.2016.0411

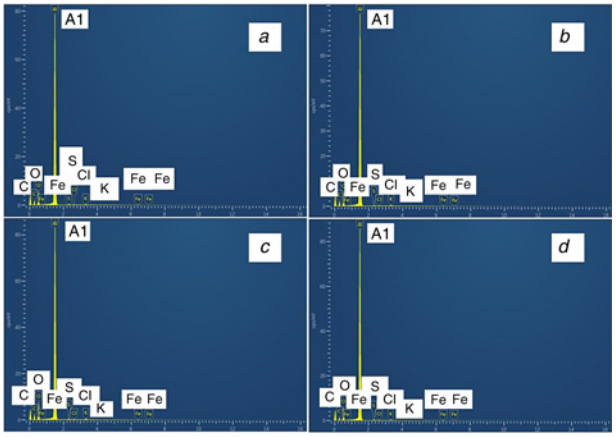

Fig. 2 *Surface of the oxide film obtained under different pulse width EDS spectrum*
a 32 μs
b 12 μs
c 6 μs
d 4 μs

energy, such as formula (1) [14]

$$E = \int_0^t u(t)i(t)\,\mathrm{d}t \tag{1}$$

wherein E is the single pulse energy, $u(t)$ is the instantaneous voltage of discharge gap, $i(t)$ is the instantaneous current of discharge gap and t is the duration time of the discharge pulse.

When the pulse width decreases, the discharge time decreases and the discharge frequency increases. So the single pulse energy decreases result with the growth rate of oxide film decreasing according to formula (1). When the pulse width decreases to a certain value, the oxide film becomes the thinnest. Then the relationship changes the tendency to rise. This phenomenon indicates that there is an ultimate thickness value of the oxide film when the pulse width changing.

3.4. Oxide film roughness and friction coefficient analysis: Measured by a Marr contourgraph, the surface roughness values of the 1060 Al and its oxide film under different pulse widths are shown as Table 4. Moreover, the relation between the roughness and the pulse widths is shown in Fig. 8. The roughness value decreases gradually with the pulse width decreasing. Moreover, we can learn that the surface roughness values of the Al_2O_3 oxide film are larger than that of 1060 Al blank surfaces because of the honeycomb structure of oxide film.

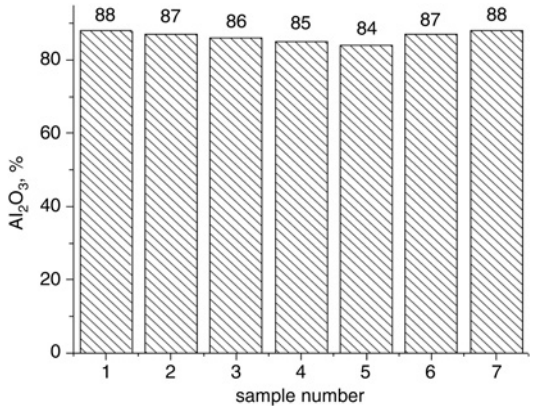

Fig. 3 *Content of Al_2O_3 in the oxide film*

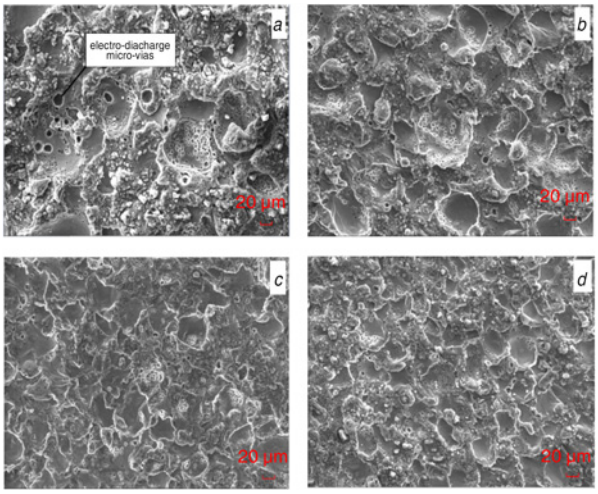

Fig. 4 *SEM images of the oxide film surfaces obtained under different pulse widths*
a 32 μs
b 12 μs
c 6 μs
d 4 μs

Finally, the nanoscratch test is done on the sample surface by using a nanoindentation. The ruling distance is 5 mm, ruling speed is 0.05 cm/s, and ruling force is 500 mN. The surface friction coefficient of the sample obtained by the test is shown in Fig. 9. The friction coefficient of 1060 Al surface is 0.172, which is larger than the values of the oxide films. With the pulse width decreasing, the oxide film friction coefficient first increases then decreases, and finally stabilise.

On the other hand, the influence of the pulse width on the friction coefficient can be turned into impact of the roughness value on the friction coefficient when the discharge energy of WEDM-HS is reached and there is a similar research trend in the literature [15], as shown in Fig. 10.

For further explain, based on the micromorphology analysis, the main reason of the above results is that the microstructure of the oxide film will reduce the actual contact area and intermolecular force of the diamond indenter to the oxide film. Moreover, the accommodation function of the honeycomb structure with

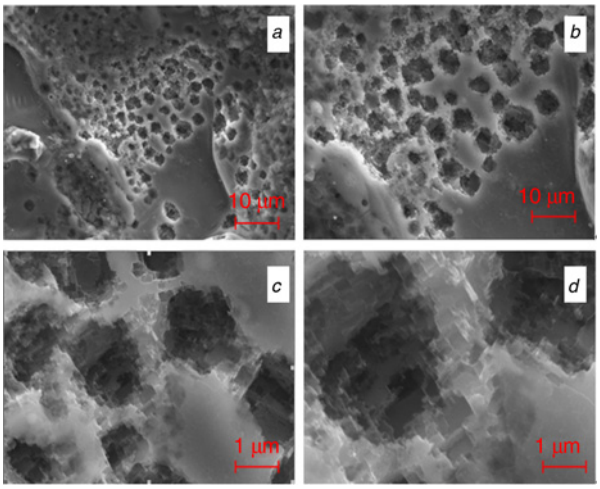

Fig. 5 *SEM images of discharge micropore under different amplification factors*
a 1 K×
b 2 K×
c 7 K×
d 15 K×

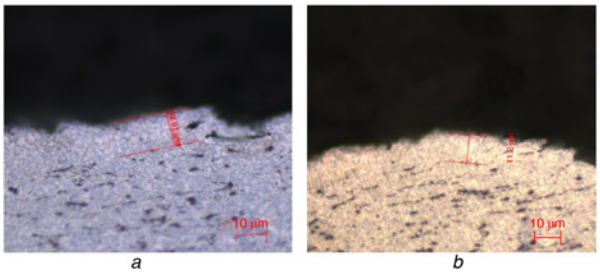

Fig. 6 *Cross-section morphology of the oxide film*
a 36 μs
b 12 μs

Table 3 Thickness of the oxide film under different pulse widths

Number	1	2	3	4	5	6	7
thickness, μm	12.9	12.1	11.5	11.2	7.7	9.2	10.1

Thickness of the oxide film (mean value) is measured by laser scanning confocal microscope

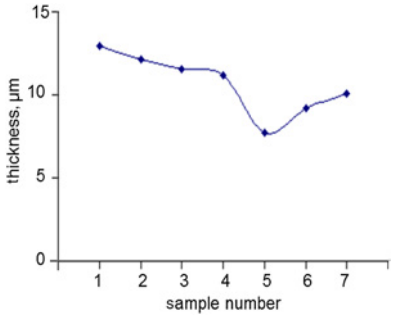

Fig. 7 *Thickness of oxide film under different pulse widths*

Table 4 Roughness values of 1060 Al and its oxide film

Sample	Ra, μm	Rz, μm	Rq, μm
1060 Al	0.204	3.143	0.355
1	6.742	8.357	36.658
2	6.260	7.870	33.527
3	5.066	6.471	30.939
4	4.786	5.992	27.348
5	3.699	4.613	26.058
6	3.095	3.929	19.023
7	2.676	3.361	17.265

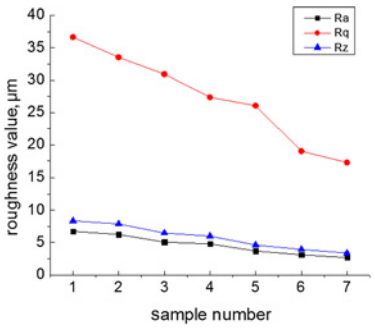

Fig. 8 *Roughness values of oxide film under different pulse widths*

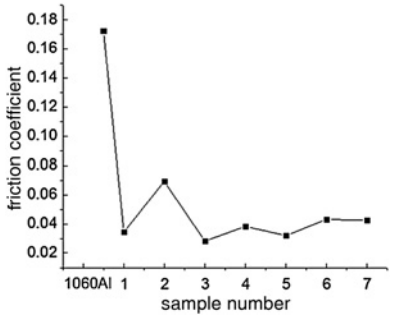

Fig. 9 *Values of friction coefficient on 1060 Al surface, (1)–(7) WEDM-HS samples 1–7*

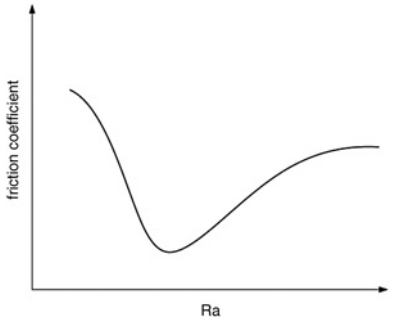

Fig. 10 *Friction coefficient against roughness value*

microholes can reduce the remaining quantity of grinding grains between the friction surfaces. So it turns out to be that there is a small friction coefficient of the oxide film, which can reduce the shear strength of the contact interface contained microparticles. Even it can change the friction process of two-body into that of three-body to reduce the friction coefficient. It effectively reduces the abrasive wear and adhesive wear, and the anti-erosion performance has been greatly improved [16, 17]. This can be regarded as the research value of this Letter for the pure Al processed by using WEDM-HS.

4. Conclusions

(i) More than 84% of the Al_2O_3 content is found in the oxide film of the 1060 pure Al processed by WEDM-HS. Moreover, the phase composition of the oxide film does not change with the pulse width decreasing.
(ii) The surface of the oxide film is composed of honeycomb holes with microns size. With the pulse width decreasing, the diameter and depth of the discharge microholes both decrease and the honeycomb structure arranges close. The ladder-like microstructures of square bracket are found for the first time at the inside wall from bottom to top of the microholes.
(iii) With the decreasing of the pulse width, the surface roughness of the oxide film decreases, and the thickness and the friction coefficient of the oxide film first decrease then increase and finally tend to be stable. They both have certain relationships with the Al_2O_3 content of the oxide film.

5. Acknowledgments: The research in this paper was sponsored by the National Science Foundation of China (grant nos. 51405031, 51575057).

6 References

[1] Zeng H.L., Yang J.C.: 'Electrolytic and chemical conversion coating' (Light Industry Press, Beijing, 1987)

doi: 10.1049/mnl.2016.0411

[2] Gao Y.X.: 'Aluminum finish' (Metallurgical Industry Press, Beijing, 1991)
[3] Sundararajan G., Krishna L.R.: 'Mechanisms underlying the formation of thick alumina coatings through the MAO coating technology', *Surf. Coat. Technol.*, 2003, **167**, pp. 269–277
[4] Xin T.Z., Zhao W.S., Liu J.C.: 'Study on tribological properties and microstructure of aluminum surface micro-arc oxidation ceramic coating', *Aerosp. Manuf. Technol.*, 2005, **4**, pp. 5–8
[5] Rakech A.G., Khokhlov V.V., Bautin V.A., *ET AL.*: 'Model concepts on the mechanism of micro arc oxidation of metal materials and control over this process', *Prot. Met.*, 2006, **42**, (2), pp. 158–169
[6] Gnedenkov S.V.: 'Composition and ad1esion of protective coating on aluminum', *Surf. Coat. Technol.*, 2000, **145**, pp. 146–151
[7] Deng Z.W.: 'Aluminum surface micro-arc oxidation technology', *Mater. Prot.*, 1996, **29**, (2), pp. 15–16
[8] Shi Y.L.: 'On the surface of the aluminum plasma micro-arc oxidation technology research', *Plat. Finish.*, 2000, **19**, (1), pp. 15–18
[9] Gao Y., Gao B., Wang R., *ET AL.*: 'Improved biological performance of low modulus Ti-24Nb-4Zr-7.9 Sn implants due to surface modification by anodic oxidation', *Appl. Surf. Sci.*, 2009, **255**, p. 5009
[10] Narayanan R., Seshadri S.K.: 'Point defect model and corrosion of anodic oxide coatings on Ti-6Al-4V', *Corros. Sci.*, 2008, **50**, p. 1521
[11] Lu Y.: 'Loading capacity of a self-assembled super hydrophobic boat array fabricated via electrochemical method', *Micro Nano Lett.*, 2012, **7**, (8), pp. 1750–0443
[12] Cui H., Guo L.B., Zhang B., *ET AL.*: 'Research on tribological properties of micro wire electrical discharge machining surface', *J. Harbin Eng. Univ.*, 2013, **34**, (10), pp. 1316–1320
[13] Cui H., Guo L.-B., Zhang B., *ET AL.*: 'Tribological property comparison between micro-WEDM and super finishing grinding machining surfaces', *J. Central South Univ. (Sci. Technol.)*, 2013, **44**, (9), pp. 3687–3692
[14] Di S.C., Huang R.N., Yu B., *ET AL.*: 'Research status and development trend of LSWEDM pulse generator', *Aviat. Prec. Manuf. Technol.*, 2004, **40**, (6), pp. 12–16
[15] Wang Z.T., Meng J.S.: 'Friction and wear and abrasion resistant materials' (Harbin Industrial University Press, Harbin, 2013)
[16] Huang C.A.: 'The surface alloying behavior of martensitic stainless steel cut with wire electrical discharge machine', *Appl. Surf. Sci.*, 2006, **8**, (252), pp. 2915–2926
[17] Chen K., Zhao W.L.: 'Study on organization and performance of nitrogen ion implantation layer of 304 austenitic stainless steel', *Surf. Tech.*, 2011, **40**, (2), pp. 18–20